Archives of Acoustics Vol. 46, No. 4, pp. 623–635 (2021), doi: 10.24425/aoa.2021.138155

Research Paper

Reflection and Transmission of Plane Wave at an Interface Between Two Rotating Micropolar Piezoelectric Solid Half-Spaces

Baljeet SINGH(1)*, Asha SANGWAN(2), Jagdish SINGH(3)

(1) *Department of Mathematics, Post Graduate Government College*
Sector 11, Chandigarh, 160011, India
*Corresponding Author e-mail: bsinghgc11@gmail.com

(2) *Department of Mathematics, Government College*
Sampla, Rohtak, 124001, Haryana, INDIA; e-mail: aashisangwan53@gmail.com

(3) *Department of Mathematics, Maharshi Dayanand University*
Rohtak, 124001, Haryana, India; e-mail: jsnandal2k15@gmail.com

(*received November 28, 2020; accepted October 6, 2021*)

In this paper, we investigate a problem on reflection and transmission of plane-waves at an interface between two dissimilar half-spaces of a transversely isotropic micropolar piezoelectric material. The entire model is assumed to rotate with a uniform angular velocity. The governing equations of rotating and transversely isotropic micropolar piezoelectric medium are specialized in a plane. Plane-wave solutions of two-dimensional coupled governing equations show the possible propagation of three coupled plane-waves. For an incident plane-wave at an interface between two dissimilar half-spaces, three reflected and three transmitted waves propagate with distinct speeds. The connections between the amplitude ratios of reflected and transmitted waves are obtained. The expressions for the energy ratios of reflected and transmitted waves are also obtained. A numerical example of the present model is considered to illustrate the effects of rotation on the speeds and energy ratios graphically.

Keywords: plane-wave; micropolar piezoelectricity; reflection and transmission; amplitude ratios; energy ratios; rotation.

1. Introduction

The reflection and transmission phenomenon of elastic waves at an interface between two different media is of great concern in many fields including composites engineering, geology, seismology, seismic exploration and acoustics. The study of propagation, reflection and transmission of plane waves plays a vital role in providing information of the internal structure of the material medium. Some classical problems on reflection and transmission of elastic waves in layered media were analysed by various authors (Knott, 1899; Jeffreys, 1926; Gutenberg, 1944; Ergin, 1950; Ewing *et al.*, 1957; Achenbach, 1973). The wave phenomenon in piezoelectric media has its applications in the generation and transmission of disturbances in electro-acoustic devices like transducers and resonators. The reflection and transmission of plane-waves in the theory of piezoelectricity have many applications in the area of signal processing, transduction and frequency control (Auld, 1981; Kaung, 2013; Parton, Kudryavtsev, 1988; Rosenbaum, 1988; Xue *et al.*, 2012). The propagation, reflection and transmission of plane waves in the piezoelectric materials were studied by Kyame (1949), Pailloux (1958), Hruska (1966), Auld (1973), Cheng and Sun (1975), Alshits *et al.* (1984), Every and Neiman (1992), Alshits and Shuvalov (1995), Pang *et al.* (2008), Darinskii *et al.* (2008), Burkov *et al.* (2009), Singh (2010), Kuang and Yuan (2011), Yuan and Zhu (2012), Singh (2013), Guo and Wei (2014), Guo *et al.* (2015), Oth-

MAN *et al.* (2017a; 2017b), JIAO *et al.* (2019), SAHU *et al.* (2021), LIU *et al.* (2021), and SINGH *et al.* (2021).

Functionally graded materials are typically created by two or more materials, which have unique characteristic properties varying gradually in a certain direction. When used with piezoelectric materials, functionally graded manufacturing methods introduce new smart materials known as functionally graded piezoelectric materials (FGPMs). The functionally graded piezoelectric models increase the efficiency and mechanical performance of piezoelectric structures. The analysis of structures made of these materials has been brought to a worldwide attention by various researchers such as BARATI and ZENKOUR (2018), ZENKOUR and ALGHANMI (2019a; 2019b; 2020), ZENKOUR and ALJADANI (2019; 2020), ZENKOUR and HAFED (2019; 2020a; 2020b), and PAL and SINGH (2021).

The micropolar elasticity is a generalization of classical elasticity with extra independent degrees of freedom for local rotation. In the micropolar theory, the particle motions are expressed in terms of displacement and micro-rotation vector. ERINGEN (1966; 1968; 1999) introduced the linear theory of micropolar elasticity and explained the micro-rotational motion and spin inertia that can support coupled stress and body couples in elastic materials. The theory of micropolar elasticity was applied to piezoelectricity by many researchers (CRACIUM, 1995; CIUMASU, VIERU, 1999; VIERU, CIUMASU, 1999; ZHILIN, KOLPAKOV, 2005; IESAN, 2006; AOUADI, 2008; GALES, 2012). Reflection and transmission coefficients are useful parameters for the quantitative characterization of the geoacoustic properties of the seabed sediment and its subbottom structure. The theory of micropolar elasticity is adequate to study the propagation of acoustics in the seabed materials. The reflection and transmission phenomenon in piezoelectric materials with micropolar effects hasn't been investigated much in literature. For example, SINGH and SINDHU (2016; 2018) studied the rotational and micro-rotational effects on wave speed of Rayleigh-wave in a micropolar piezoelectric medium. SANGWAN *et al.* (2018) studied the reflection and transmission of elastic waves at an interface between an elastic half-space and a micropolar piezoelectric half-space. SINGH *et al.* (2019) studied the reflection and transmission of elastic wave at an interface between two micropolar piezoelectric half-spaces.

The translation and rotation of a moving object can be sensed by accelerometers and gyroscopes, respectively. These motion sensors are used as an important tool in smart weapon systems, video cameras, automobiles, robotics, navigation and machine control. Recently, vibratory gyroscopes made up of piezoelectric materials have become a center of interest in many researches. The equations of motions for a rotating piezoelectric body with Coriolis and centrifugal accelerations are responsible for observing the fundamental nature of the piezoelectric gyroscope. SCHOENBERG and CENSOR (1973) studied the effect of rotation on plane wave propagation in an isotropic medium. The effects of rotation on frequency or wave speed provide valuable inputs for the design of acoustic sensors (WHITE, 1998). In particular, the rotation induced frequency shifts have been applied to manufacture the gyroscopes (TIERSTEN *et al.*, 1980; 1981; WREN, BURDESS, 1987).

The main purpose of the present paper is to illustrate the effect of rotation on the reflection and transmission phenomenon of plane-waves at a welded interface between two different transversely isotropic micropolar piezoelectric solid half-spaces. The present paper is organized as follows: in Sec. 2 the governing equations for linear rotating micropolar piezoelectric materials are formulated and specialized in x-z-plane. Plane-wave solutions of the specialized equations are obtained in Sec. 3. In Sec. 4 two different half-spaces of micropolar piezoelectric material are assumed in welded contact to study the reflection and transmission of plane-waves. The connections between the amplitudes of the incident, reflected and transmitted waves are obtained. The expressions for the energy ratios of reflected and transmitted waves are also derived. In Sec. 5, the speeds and energy ratios of reflected and transmitted waves are computed for a given model and are illustrated graphically to observe the rotational effects.

2. Governing equations

We assume that the micropolar piezoelectric solid rotates uniformly with an angular velocity $\mathbf{\Omega} = \Omega\widehat{n}$ where Ω is rotation parameter and $\widehat{n}$ is a unit vector representing the direction of the axis of rotation. The fixed coordinate system in the rotating micropolar piezoelectric medium introduces additional terms in the equations of motion: centripetal acceleration is $\mathbf{\Omega} \times (\mathbf{\Omega} \times \mathbf{u})$ due to time varying motion only and $(2\mathbf{\Omega} \times \dot{\mathbf{u}})$ is the Coriolis acceleration, where $\mathbf{u}$ is the displacement vector. Following AOUADI (2008) and SCHOENBERG and CENSOR (1973), the governing field equations for the linear theory of rotating micropolar piezoelectric solids in the absence of body forces and body couples are:

(a) equations of motion

$$\sigma_{ji,j} = \rho\left[\ddot{u}_i + \{\mathbf{\Omega} \times (\mathbf{\Omega} \times \mathbf{u})\}_i + (2\mathbf{\Omega} \times \dot{\mathbf{u}})_i\right], \tag{1}$$

$$m_{ik,i} + \varepsilon_{ijk}\sigma_{ij} = \rho j\ddot{\phi}_k, \tag{2}$$

(b) electric field equations

$$D_{j,j} = q_e E_k = -\psi_{,k}, \tag{3}$$

(c) the constitutive equations

$$\sigma_{ij} = c_{ijkl}e_{kl} + b_{ijkl}\kappa_{kl} + \lambda_{ijk}E_k, \tag{4}$$

$$m_{ij} = b_{klij}e_{kl} + a_{ijkl}\kappa_{kl} + \beta_{ijk}E_k, \tag{5}$$

$$D_k = -\lambda_{ijk}e_{ij} - \beta_{ijk}\kappa_{ij} + \gamma_{kj}E_j, \tag{6}$$

(d) the geometrical equations

$$e_{ij} = u_{j,i} + \varepsilon_{ijk}\phi_k, \qquad \kappa_{ij} = \phi_{j,i}, \tag{7}$$

where σ_{ij} is the stress tensor, ρ is the mass density, $\boldsymbol{\phi}$ is the microrotation vector, j is the micro-inertia, m_{ij} is the couple stress tensor, ε_{ijk} is the alternating symbol, D_k is the dielectric displacement vector, q_e is the volume charge density, E_j is the electric field vector, ψ is the electrostatic potential, e_{ij} and κ_{ij} are kinematic strain measures and a_{ijkl}, b_{ijkl}, c_{ijkl}, λ_{ijk}, β_{ijk}, and γ_{jk} are constitutive coefficients. Superposed dot denotes partial differentiation with respect to the time t. Subscripts preceded by a comma denote partial differentiation with respect to the corresponding Cartesian coordinate and the repeated index in the subscript implies summation. The constitutive coefficients satisfy the following symmetry relations

$$c_{ijkl} = c_{klij}, \qquad a_{ijkl} = a_{klij}, \qquad \gamma_{ij} = \gamma_{ji}. \tag{8}$$

We consider two dissimilar linear, homogeneous transversely isotropic rotating micropolar piezoelectric half-spaces in welded contact. The origin of the Cartesian coordinate system (x, y, z) is taken on the plane interface and z-axis pointing vertically downwards into rotating micropolar piezoelectric half-space ($z \geq 0$). The upper half-space ($z \leq 0$) and lower half-space ($z \geq 0$) are denoted by M' and M, respectively. All quantities in medium M' are denoted by a superposed prime. We assume that the medium is transversely isotropic in such a way that the plane of isotropy is perpendicular to z-axis. For two-dimensional motion in x-z-plane, we consider the following components of the displacement vector $\mathbf{u}$ and microrotation vector $\boldsymbol{\phi}$

$$\mathbf{u} = (u_1, 0, u_3), \qquad \boldsymbol{\phi} = (0, \phi_2, 0). \tag{9}$$

Making use of Eqs (1)–(9), the following governing equations of motion in x-z-plane are obtained for a transversely isotropic and rotating micropolar piezoelectric medium

$$\begin{aligned} A_{11}\frac{\partial^2 u_1}{\partial x^2} &+ (A_{13} + A_{56})\frac{\partial^2 u_3}{\partial x \partial z} + A_{55}\frac{\partial^2 u_1}{\partial z^2} \\ &+ K_1\frac{\partial \phi_2}{\partial z} - (\lambda_{15} + \lambda_{31})\frac{\partial^2 \psi}{\partial x \partial z} \\ &= \rho\left[\frac{\partial^2 u_1}{\partial t^2} - \Omega^2 u_1 + 2\Omega\frac{\partial u_3}{\partial t}\right], \end{aligned} \tag{10}$$

$$\begin{aligned} A_{66}\frac{\partial^2 u_3}{\partial x^2} &+ (A_{13} + A_{56})\frac{\partial^2 u_1}{\partial x \partial z} + A_{33}\frac{\partial^2 u_3}{\partial z^2} \\ &+ K_2\frac{\partial \phi_2}{\partial x} - \lambda_{15}\frac{\partial^2 \psi}{\partial x^2} - \lambda_{33}\frac{\partial^2 \psi}{\partial z^2} \\ &= \rho\left[\frac{\partial^2 u_3}{\partial t^2} - \Omega^2 u_3 - 2\Omega\frac{\partial u_1}{\partial t}\right], \end{aligned} \tag{11}$$

$$\begin{aligned} B_{77}\frac{\partial^2 \phi_2}{\partial x^2} &+ B_{66}\frac{\partial^2 \phi_2}{\partial z^2} - \chi\phi_2 - K_1\frac{\partial u_1}{\partial z} \\ &- K_2\frac{\partial u_3}{\partial x} = \rho j\frac{\partial^2 \phi_2}{\partial t^2}, \end{aligned} \tag{12}$$

$$\begin{aligned} \lambda_{15}\frac{\partial^2 u_3}{\partial x^2} &+ \lambda_{33}\frac{\partial^2 u_3}{\partial z^2} + (\lambda_{15} + \lambda_{31})\frac{\partial^2 u_1}{\partial x \partial z} \\ &+ \gamma_{11}\frac{\partial^2 \psi}{\partial x^2} + \gamma_{33}\frac{\partial^2 \psi}{\partial z^2} = 0, \end{aligned} \tag{13}$$

where $A_{11} = C_{1111}$, $A_{55} = C_{3131}$, $A_{13} = C_{1133} = C_{3311}$, $A_{56} = C_{3113} = C_{1331}$, $A_{66} = C_{1313}$, $A_{33} = C_{3333}$, $K_1 = A_{56} - A_{55} = C_{3113} - C_{3131}$, $K_2 = A_{66} - A_{56} = C_{1313} - C_{1331}$, $\chi = K_2 - K_1$, $B_{77} = a_{1212}$, $B_{66} = a_{3232}$, $\lambda_{31} = \lambda_{311}$, $\lambda_{33} = \lambda_{333}$, $\lambda_{15} = \lambda_{131} = \lambda_{113}$, $\lambda_{35} = \lambda_{313} = \lambda_{331}$.

3. Plane-waves

We consider the plane-waves in the x-z-plane with a wave front parallel to the y-axis. We seek the following plane-wave solutions of Eqs (10)–(13)

$$\begin{aligned} \{u_1, u_3, \phi_2, \psi\} &= (A, B, C, D) \\ &\cdot \exp\{ik(x\sin\theta + z\cos\theta) - i\omega t\}, \end{aligned} \tag{14}$$

where k is the wavenumber, $\omega = kv$ is the circular frequency and v is the speed of wave propagating in x-z-plane along a direction making an angle θ with z-axis.

Using Eq. (14) in Eqs (10)–(13), we obtain a homogeneous system of four equations in A, B, C, and D which have a non-trivial solution if

$$H_0\Lambda^3 - H_1\Lambda^2 + H_2\Lambda - H_3 = 0, \tag{15}$$

where $\Lambda = \left(\frac{v}{\omega}\right)^2$ and H_0, H_1, H_2, H_3 are given in Appendix 1.

The three real roots v_1, v_2 and v_3 ($v_1 > v_2 > v_3$) of Eq. (15) correspond to the speeds of propagation of Coupled Longitudinal Displacement (CLD), Coupled Transverse Displacement (CTD), and Coupled Transverse Microrotational (CTM) waves, respectively. In the absence of piezoelectric and transverse isotropy, the velocity Eq. (15) agrees with (Parafitt, Eringen, 1969).

4. Reflection and transmission

A plane coupled longitudinal displacement (CLD) wave propagating with velocity v_1' through the transversely isotropic rotating micropolar piezoelectric solid half-space (M') is considered as incident wave at the interface $z = 0$ making an angle θ_o with negative z-axis. The incident CLD wave generates three reflected CLD, CTD and CTM waves of amplitude A_m' ($m = 1, 2, 3$) propagating with speeds v_m' ($m = 1, 2, 3$) in medium M'

and three transmitted CLD, CTD and CTM waves of amplitude A_m $(m = 1,2,3)$ propagating with speeds v_m $(m = 1,2,3)$ in medium M. The geometry showing the directions of propagation of incident, reflected and transmitted waves is shown in Fig. 1. The appropriate displacement components u_1', u_3', microrotation component ϕ_2' and electric potential ψ' for incident and reflected waves in medium M' are

$$u_1' = A_o \exp\{ik_1'(x\sin\theta_o + z\cos\theta_o) - i\omega t\} + \sum_{m=1}^{3} A_m' \exp\{ik_m'(x\sin\theta_m' - z\cos\theta_m') - i\omega t\}, \quad (16)$$

$$u_3' = \xi_o A_o \exp\{ik_1'(x\sin\theta_o + z\cos\theta_o) - i\omega t\} + \sum_{m=1}^{3} \xi_m' A_m' \exp\{ik_m'(x\sin\theta_m' - z\cos\theta_m') - i\omega t\}, \quad (17)$$

$$\phi_2' = \eta_o A_o \exp\{ik_1'(x\sin\theta_o + z\cos\theta_o) - i\omega t\} + \sum_{m=1}^{3} \eta_m' A_m' \exp\{ik_m'(x\sin\theta_m' - z\cos\theta_m') - i\omega t\}, \quad (18)$$

$$\psi' = \zeta_o A_o \exp\{ik_1'(x\sin\theta_o + z\cos\theta_o) - i\omega t\} + \sum_{m=1}^{4} \zeta_m' A_m' \exp\{ik_m'(x\sin\theta_m' - z\cos\theta_m') - i\omega t\}, \quad (19)$$

and the appropriate displacement components u_1, u_3, microrotation component ϕ_2, electric potential ψ for transmitted waves in medium M are

$$u_1 = \sum_{m=1}^{3} A_m \exp\{ik_m(x\sin\theta_m + z\cos\theta_m) - i\omega t\}, \quad (20)$$

$$u_3 = \sum_{m=1}^{3} \xi_m A_m \exp\{ik_m(x\sin\theta_m + z\cos\theta_m) - i\omega t\}, \quad (21)$$

$$\phi_2 = \sum_{m=1}^{3} \eta_m A_m \exp\{ik_m(x\sin\theta_m + z\cos\theta_m) - i\omega t\}, \quad (22)$$

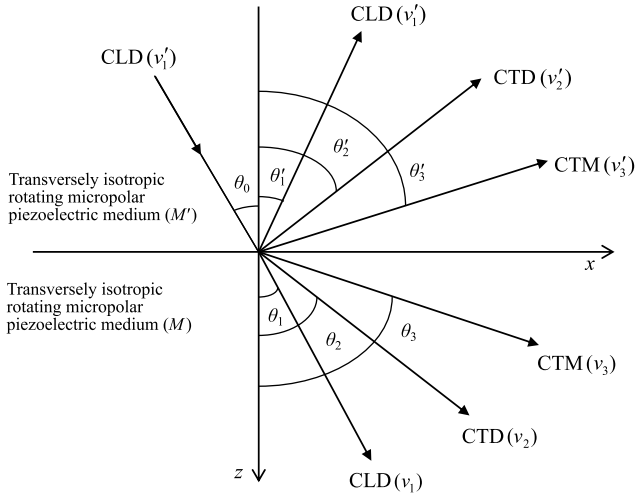

Fig. 1. Geometry of the problem showing incident, reflected and transmitted waves.

$$\psi = \sum_{j=1}^{3} \zeta_m A_m \exp\{ik_m(x\sin\theta_m + z\cos\theta_m) - i\omega t\}, \quad (23)$$

where v_m' $(m = 1,2,3)$ are the real speeds of reflected CLD, CTD and CTM waves respectively in medium M' and v_m $(m = 1,2,3)$ are the real speeds of transmitted CLD, CTD, and CTM waves respectively in medium M, and the explicit expressions for coupling coefficients ξ_o, η_o, ζ_o, ξ_m', η_m', ζ_m', ξ_m, η_m, and ζ_m $(m = 1,2,3)$ are listed in Appendix 2.

The relevant boundary conditions at the interface $z = 0$ are the continuity of normal and tangential force stress components, tangential couple stress components, electric displacement, electric potential and normal displacement components, which are written as

$$\begin{aligned} &\sigma_{33} = \sigma_{33}', \qquad \sigma_{31} = \sigma_{31}', \qquad D_3 = D_3', \\ &m_{32} = m_{32}', \qquad \psi = \psi', \qquad u_3 = u_3', \end{aligned} \quad (24)$$

where

$$\begin{aligned} \sigma_{33}' &= A_{13}'\frac{\partial u_1'}{\partial x} + A_{33}'\frac{\partial u_3'}{\partial z} - \lambda_{35}'\frac{\partial \psi'}{\partial x} - \lambda_{33}'\frac{\partial \psi'}{\partial z}, \\ \sigma_{33} &= A_{13}\frac{\partial u_1}{\partial x} + A_{33}\frac{\partial u_3}{\partial z} - \lambda_{35}\frac{\partial \psi}{\partial x} - \lambda_{33}\frac{\partial \psi}{\partial z}, \\ \sigma_{31}' &= A_{56}'\frac{\partial u_3'}{\partial x} + A_{55}'\frac{\partial u_1'}{\partial z} + (A_{56}' - A_{55}')\phi_2' - \lambda_{31}'\frac{\partial \psi'}{\partial x} - \lambda_{35}'\frac{\partial \psi'}{\partial z}, \\ \sigma_{31} &= A_{56}\frac{\partial u_3}{\partial x} + A_{55}\frac{\partial u_1}{\partial z} + (A_{56} - A_{55})\phi_2 - \lambda_{31}\frac{\partial \psi}{\partial x} - \lambda_{35}\frac{\partial \psi}{\partial z}, \\ D_3' &= \lambda_{15}'\frac{\partial u_1'}{\partial x} + \lambda_{33}'\frac{\partial u_3'}{\partial z} + \gamma_{33}'\frac{\partial \psi'}{\partial z}, \\ D_3 &= \lambda_{15}\frac{\partial u_1}{\partial x} + \lambda_{33}\frac{\partial u_3}{\partial z} + \gamma_{33}\frac{\partial \psi}{\partial z}, \\ m_{32}' &= B_{66}'\frac{\partial \phi_2'}{\partial z}, \\ m_{32} &= B_{66}\frac{\partial \phi_2}{\partial z}. \end{aligned}$$

The displacement components, microrotation components, and electric potentials given by Eqs (16)–(23) satisfy boundary conditions (24) under the following conditions analogous to Snell's law

$$\begin{aligned} k_1'\sin\theta_o &= k_1'\sin\theta_1' = k_2'\sin\theta_2' = k_3'\sin\theta_3' = k_1\sin\theta_1 \\ &= k_2\sin\theta_2 = k_3\sin\theta_3, \end{aligned} \quad (25)$$

$$\begin{aligned} k_1'v_1' &= k_2'v_2' = k_3'v_3' = k_4'v_4' = k_1v_1 = k_2v_2 \\ &= k_3v_3 = k_4v_4 = \omega, \end{aligned} \quad (26)$$

and we obtain the following non-homogeneous system of six equations in amplitude ratios of reflected and transmitted waves as

$$\sum_{m=1}^{6} \alpha_{pm} Z_m = \delta_p \quad (p = 1, 2, ..., 6), \tag{27}$$

where

$$Z_m = \begin{cases} \dfrac{A'_m}{A_0} & (m = 1, 2, 3), \\ \dfrac{A_{m-3}}{A_0} & (m = 4, 5, 6), \end{cases}$$

are amplitude ratios of reflected CLD wave, reflected CTD wave, reflected CTM wave, transmitted CLD wave, transmitted CTD wave, and transmitted CTM wave, respectively, and

$$\alpha_{1m} = \begin{cases} \dfrac{-\left[\left(A'_{13}-\lambda'_{35}\zeta'_m\right)\sin\theta_o-\left(A'_{33}\xi'_m-\lambda'_{33}\zeta'_m\right)a^*\right]}{\left(A'_{13}-\lambda'_{35}\zeta_o\right)\sin\theta_o+\left(A'_{33}\xi_o-\lambda'_{33}\zeta_o\right)\cos\theta_o} & (m = 1, 2, 3), \\ \dfrac{\left(A_{13}-\lambda_{35}\zeta_{m-3}\right)\sin\theta_o+\left(A_{33}\xi_{m-3}-\lambda_{33}\zeta_{m-3}\right)b^*}{\left(A'_{13}-\lambda'_{35}\zeta_o\right)\sin\theta_o+\left(A'_{33}\xi_o-\lambda'_{33}\zeta_o\right)\cos\theta_o} & (m = 4, 5, 6), \end{cases}$$

$$\alpha_{2m} = \begin{cases} \dfrac{-\left[\left(A'_{56}\xi'_m-\lambda'_{31}\zeta'_m\right)\sin\theta_o-c^*\right]}{\left(A'_{56}\xi_o-\lambda'_{31}\zeta_o\right)\sin\theta_o+\left(A'_{55}-\lambda'_{35}\zeta_o\right)\cos\theta_o-i\left(A'_{56}-A'_{55}\right)\left(\frac{\eta_o}{k'_1}\right)} & (m = 1, 2, 3), \\ \dfrac{\left(A_{56}\xi_{m-3}-\lambda_{31}\zeta_{m-3}\right)\sin\theta_o+d^*}{\left(A'_{56}\xi_o-\lambda'_{31}\zeta_o\right)\sin\theta_o+\left(A'_{55}-\lambda'_{35}\zeta_o\right)\cos\theta_o-i\left(A'_{56}-A'_{55}\right)\left(\frac{\eta_o}{k'_1}\right)} & (m = 4, 5, 6), \end{cases}$$

$$\alpha_{3m} = \begin{cases} \dfrac{-\left[\lambda'_{15}\sin\theta_o-\left(\lambda'_{33}\xi'_m+\gamma'_{33}\zeta'_m\right)\sqrt{\left(\frac{v'_1}{v'_m}\right)^2-\sin^2\theta_o}\right]}{\lambda'_{15}\sin\theta_o+\left(\lambda'_{33}\xi_o+\gamma'_{33}\zeta_o\right)\cos\theta_o} & (m = 1, 2, 3), \\ \dfrac{\lambda_{15}\sin\theta_o+\left(\lambda_{33}\xi_{m-3}+\gamma_{33}\zeta_{m-3}\right)\sqrt{\left(\frac{v'_1}{v_{m-3}}\right)^2-\sin^2\theta_o}}{\lambda'_{15}\sin\theta_o+\left(\lambda'_{33}\xi_o+\gamma'_{33}\zeta_o\right)\cos\theta_o} & (m = 4, 5, 6), \end{cases}$$

$$\alpha_{4m} = \begin{cases} \dfrac{\left(\frac{\eta'_m}{k'_m}\right)\left(\frac{v'_1}{v'_m}\right)\sqrt{\left(\frac{v'_1}{v'_m}\right)^2-\sin^2\theta_o}}{\left(\frac{\eta_o}{k'_1}\right)\cos\theta_o} & (m = 1, 2, 3), \\ \dfrac{B_{66}\left(\frac{\eta_{m-3}}{k_{m-3}}\right)\left(\frac{v'_1}{v_{m-3}}\right)\sqrt{\left(\frac{v'_1}{v_{m-3}}\right)^2-\sin^2\theta_o}}{B'_{66}\left(\frac{\eta_o}{k'_1}\right)\cos\theta_o} & (m = 4, 5, 6), \end{cases}$$

$$\alpha_{5m} = \begin{cases} \dfrac{-\zeta'_m}{\zeta_o} & (m = 1, 2, 3), \\ \dfrac{\zeta_{m-3}}{\zeta_o} & (m = 4, 5, 6), \end{cases}$$

$$\alpha_{6m} = \begin{cases} \dfrac{-\xi'_m}{\xi_o} & (m = 1, 2, 3), \\ \dfrac{\xi_{m-3}}{\xi_o} & (m = 4, 5, 6), \end{cases}$$

$\delta_p = 1 \ \ (p = 1, 2, ..., 6)$, where

$$a^* = \sqrt{\left(\frac{v'_1}{v'_m}\right)^2 - \sin^2\theta_o}, \qquad b^* = \sqrt{\left(\frac{v'_1}{v_{m-3}}\right)^2 - \sin^2\theta_o},$$

$$c^* = \left(A'_{55} - \lambda'_{35}\zeta'_m\right)\sqrt{\left(\frac{v'_1}{v'_m}\right)^2 - \sin^2\theta_o} - i\left(A'_{56} - A'_{55}\right)\left(\frac{v'_1}{v'_m}\right)\left(\frac{\eta'_m}{k'_m}\right),$$

$$d^* = \left(A_{55} - \lambda_{35}\zeta_{m-3}\right)\sqrt{\left(\frac{v'_1}{v_{m-3}}\right)^2 - \sin^2\theta_o} - i\left(A_{56} - A_{55}\right)\left(\frac{v'_1}{v_{m-3}}\right)\left(\frac{\eta_{m-3}}{k_{m-3}}\right).$$

Following (ACHENBACH, 1973), the rate of energy transmission at the interface $z = 0$ is

$$P^* = \begin{cases} \sigma'_{33}\dfrac{\partial u'_3}{\partial t} + \sigma'_{31}\dfrac{\partial u'_1}{\partial t} + m'_{32}\dfrac{\partial \phi'_2}{\partial t} & \text{for medium } M', \\ \sigma_{33}\dfrac{\partial u_3}{\partial t} + \sigma_{31}\dfrac{\partial u_1}{\partial t} + m_{32}\dfrac{\partial \phi_2}{\partial t} & \text{for medium } M. \end{cases} \tag{28}$$

The ratio of the time rate of average energy transmission for the respective reflected or transmitted waves to that of the incident wave, denoted by E_m $(m = 1, 2, ..., 6)$ for reflected CLD, reflected CTD, reflected CTM, transmitted CLD, transmitted CTD, and transmitted CTM waves respectively, are given as

$$E_m = \frac{\langle P^*_m \rangle}{\langle P^*_0 \rangle} \quad (m = 1, 2, ..., 6), \tag{29}$$

where $\langle P^*_0 \rangle$ denotes the average energy transmission per unit surface area per unit time for incident CLD wave in rotating micropolar piezoelectric medium M'.

The expressions for energy ratios at an interface $z = 0$ are given as

$$E_m = \begin{cases} \left(\dfrac{\hbar'_{1m}+\hbar'_{2m}+\hbar'_{3m}}{\hbar_o}\right) Z_m^2 & (m = 1, 2, 3), \\ \left(\dfrac{\hbar_{1m}+\hbar_{2m}+\hbar_{3m}}{\hbar_o}\right) Z_m^2 & (m = 4, 5, 6), \end{cases} \tag{30}$$

where

$$\hbar'_{1m} = \left(A'_{13}\xi'_m + A'_{56}\xi'_m - \lambda'_{35}\xi'_m\zeta'_m - \lambda'_{31}\zeta'_m\right)\sin\theta_o,$$

$$\hbar'_{2m} = -\left(A'_{55} + A'_{33}\xi'^2_m - \lambda'_{33}\xi'_m\zeta'_m - \lambda'_{35}\zeta'_m + B'_{66}\eta'^2_m\right) \cdot\sqrt{\left(\frac{v'_1}{v'_m}\right)^2 - \sin^2\theta_o},$$

$$\hbar'_{3m} = -i\left(A'_{56} - A'_{55}\right)\left(\frac{v'_1}{v'_m}\right)\left(\frac{\eta'_m}{k'_m}\right),$$

$$\hbar_o = \left(A'_{13}\xi_o + A'_{56}\xi_o - \lambda'_{35}\xi_o\zeta_o - \lambda'_{31}\zeta_o\right)\sin\theta_o + \left(A'_{55} + A'_{33}\xi_o^2 - \lambda'_{33}\xi_o\zeta_o - \lambda'_{35}\zeta_o + B'_{66}\eta_o^2\right)\cos\theta_o - i\left(A'_{56} - A'_{55}\right)\left(\frac{\eta_o}{k'_1}\right),$$

$$\hbar_{1m} = \left(A_{13}\xi_{m-3} + A_{56}\xi_{m-3} - \lambda_{35}\xi_{m-3}\zeta_{m-3} - \lambda_{31}\zeta_{m-3}\right)\sin\theta_o,$$

$$\hbar_{2m} = \Big(A_{55} + A_{33}\xi_{m-3}^2 - \lambda_{33}\xi_{m-3}\zeta_{m-3} - \lambda_{35}\zeta_{m-3} + B_{66}\eta_{m-3}^2\Big)\sqrt{\left(\frac{v_1'}{v_{m-3}}\right)^2 - \sin^2\theta_o},$$

$$\hbar_{3m} = -i\,(A_{56} - A_{55})\left(\frac{v_1'}{v_{m-3}}\right)\left(\frac{\eta_{m-3}}{k_{m-3}}\right).$$

5. Numerical results and discussion

The experimental values of physical constants of a transversely isotropic rotating micropolar piezoelectric material have not been investigated yet. In the present model, the numerical simulations of the speeds and energy ratios are restricted to a quantitative example with arbitrary physical constants for both the half-spaces (Singh, Sindhu, 2018):

- for lower half-space (M):

$A_{11} = 17.8\cdot10^{10}$ N/m^2, $A_{33} = 18.43\cdot10^{10}$ N/m^2,

$A_{13} = 7.59\cdot10^{10}$ N/m^2, $A_{56} = 1.89\cdot10^{10}$ N/m^2,

$A_{55} = 4.357\cdot10^{10}$ N/m^2, $A_{66} = 4.42\cdot10^{10}$ N/m^2,

$B_{77} = 0.278\cdot10^{9}$ N, $B_{66} = 0.268\cdot10^{9}$ N,

$\lambda_{15} = 0.00001$ C/m^2, $\lambda_{31} = 3.9$ C/m^2,

$\lambda_{33} = 1.33$ C/m^2, $\lambda_{35} = 0.23$ C/m^2,

$\gamma_{11} = 85.2$ C^2/(N$\cdot$m^2), $\gamma_{33} = 28.7$ C^2/(N$\cdot$m^2),

$\rho = 1.74\cdot10^{3}$ kg/m^3, $j = 0.196$ m^2,

$\omega = 10^{5}$ Hz,

- for upper half-space (M'):

$A'_{11} = 16.8\cdot10^{10}$ N/m^2, $A'_{33} = 17.43\cdot10^{10}$ N/m^2,

$A'_{13} = 7.2\cdot10^{10}$ N/m^2, $A'_{56} = 1.29\cdot10^{10}$ N/m^2,

$A'_{55} = 4.157\cdot10^{10}$ N/m^2, $A'_{66} = 4.1\cdot10^{10}$ N/m^2,

$B'_{77} = 0.266\cdot10^{9}$ N, $B'_{66} = 0.255\cdot10^{9}$ N,

$\lambda'_{15} = 0.000004$ C/m^2, $\lambda'_{31} = 1.75$ C/m^2,

$\lambda'_{33} = 1.23$ C/m^2, $\lambda'_{35} = 0.22$ C/m^2,

$\gamma'_{11} = 82.3$ C^2/(N$\cdot$m^2), $\gamma'_{33} = 25.7$ C^2/(N$\cdot$m^2),

$\rho' = 1.2\cdot10^{3}$ kg/m^3, $j' = 0.192$ m^2.

Using Eqs (15)–(27), and (30), a program in MATLAB software was developed. For the above physical parameters, the speeds of plane-waves, the amplitude ratios and the energy ratios of various reflected and transmitted waves were computed for different values of rotation rate $\Omega^*(=\Omega/\omega)$.

5.1. Speeds of plane-waves

The speeds of reflected CLD, CTD, CTM and transmitted CLD, CTD and CTM waves are plotted in Figs 2–7 against the incident angle θ_o. The black, red, and green curves in Figs 2–7 correspond to the speeds of various reflected and transmitted waves for $\Omega^* = 0, 0.1$, and 0.2, respectively.

Figure 2 demonstrates the speed variations of reflected CLD waves against the angle of incidence. In the absence of rotation ($\Omega^* = 0$), the speed of the reflected CLD wave, as shown by black curve, decreases monotonically from a value $1.2052\cdot10^4$ ms^{-1} at $\theta_o = 0^o$ to its minimum value $1.1126\cdot10^4$ ms^{-1} at $\theta_o = 47°$. Thereafter, it increases monotonically to a value $1.1832\cdot10^4$ ms^{-1} at $\theta_o = 90°$. In the presence of rotation (i.e. for $\Omega^* = 0.1$ and 0.2), the speed variations of CLD waves are similar to that for $\Omega^* = 0$, but the values of the speed enhance at each incident angle.

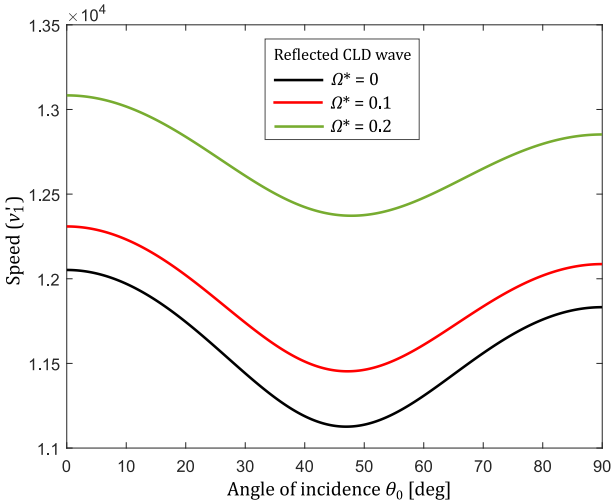

Fig. 2. The speed variations of reflected coupled longitudinal displacement (CLD) wave against the angle of incidence of incident CLD wave for different values of rotation rate.

The speed variations of reflected CTD waves against the angle of incidence are illustrated in Fig. 3. In the absence of rotation ($\Omega^* = 0$), the speed of the reflected CTD wave as shown by black curve increases monotonically from a value $5.9124\cdot10^3$ ms^{-1} at $\theta_o = 0°$ to its maximum value $7.3092\cdot10^3$ ms^{-1} at $\theta_o = 45°$. Beyond $\theta_o = 45°$, the speed decreases monotonically to a value $5.8711\cdot10^3$ ms^{-1} at $\theta_o = 90°$. In the absence of rotation (i.e. for $\Omega^* = 0.1$ and 0.2), the speed variations of CTD waves are observed similar to that for $\Omega^* = 0$, but the values of the speed drop at each incident angle.

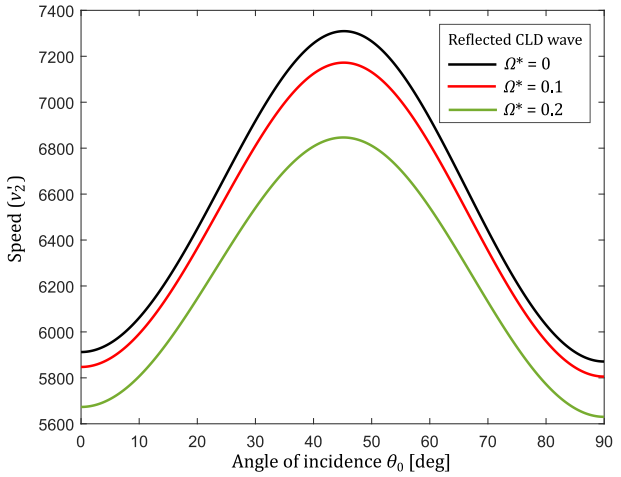

Fig. 3. The speed variations of reflected coupled transverse displacement (CTD) wave against the angle of incidence of incident CLD wave for different values of rotation rate.

The speed variations of reflected CTM waves against the angle of incidence are shown graphically in Fig. 4. In the absence of rotation, the speed of the reflected CTM wave, as shown by black curve, increases monotonically from a value $1.0604 \cdot 10^3$ ms^{-1} at $\theta_o = 0°$ to its maximum value $1.0832 \cdot 10^3$ ms^{-1} at $\theta_o = 90°$. In the presence of rotation (i.e. for $\Omega^* = 0.1$ and 0.2), the speed variations of CTM waves are found similar to those for $\Omega^* = 0$ with very little changes at each incident angle.

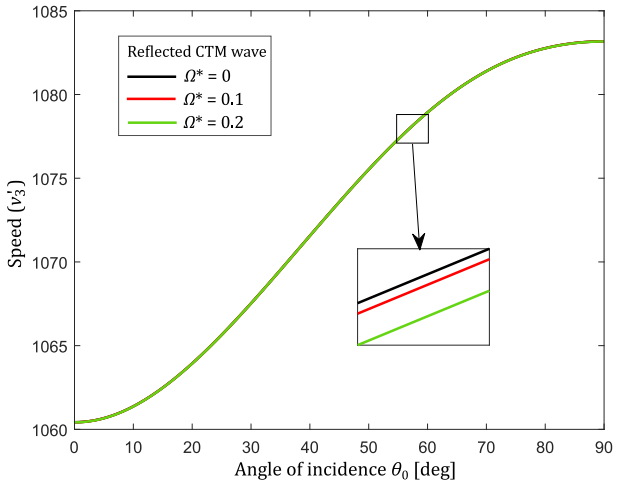

Fig. 4. The speed variations of reflected coupled transverse microrotational (CTM) wave against the angle of incidence of incident CLD wave for different values of rotation rate.

The speed variations of transmitted CLD, CTD and CTM waves are illustrated graphically against the angle of incidence in Figs 5–7, which are found similar to those for reflected CLD, CTD, and CTM waves, respectively. The dependence of transmitted wave speeds on the rotation rate is also observed similar to those for reflected wave speeds.

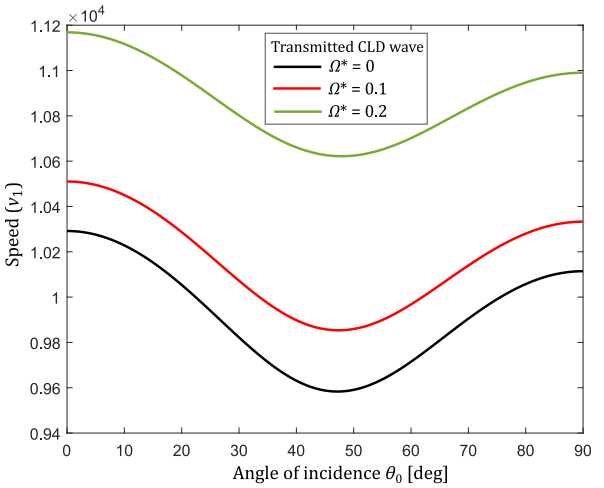

Fig. 5. The speed variations of transmitted coupled longitudinal displacement (CLD) wave against the angle of incidence of incident CLD wave for different values of rotation rate.

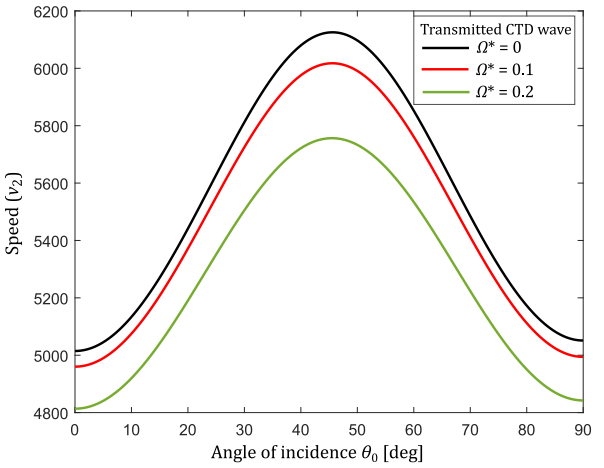

Fig. 6. The speed variations of transmitted coupled transverse displacement (CTD) wave against the angle of incidence of incident CLD wave for different values of rotation rate.

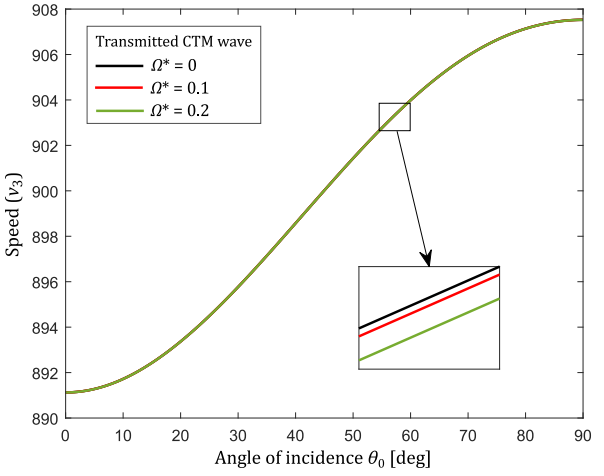

Fig. 7. The speed variations of transmitted coupled transverse microrotational (CTM) wave against the angle of incidence of incident CLD wave for different values of rotation rate.

5.2. Energy ratios of reflected and transmitted waves

The energy ratios $|E_i|$ $(i = 1, 2, ..., 6)$ of reflected and transmitted CLD, CTD, and CTM waves are illustrated graphically in Figs 8–13 for the range $0° < \theta_o < 90°$ of the angle of incidence of CLD wave for different values of rotation rate, i.e. $\Omega^* = 0.1$ (black curve), $\Omega^* = 0.2$ (red curve), and $\Omega^* = 0.3$ (green curve).

Figure 8 illustrates the energy ratio variations of reflected CLD waves against the angle of incidence for different values of rotation rate. For each value of rotation rate, these energy ratio variations oscillate till $\theta_o = 70°$ and then they increase exponentially to a maximum value one at grazing incidence. The energy ratio variations of reflected CTD and CTM waves are shown graphically in Figs 9 and 10 against the angle of incidence for different values of rotation rate. For each value of rotation rate, the energy ratios for these waves are zero at normal and grazing angles and oscillate in range between normal incidence and grazing incidence.

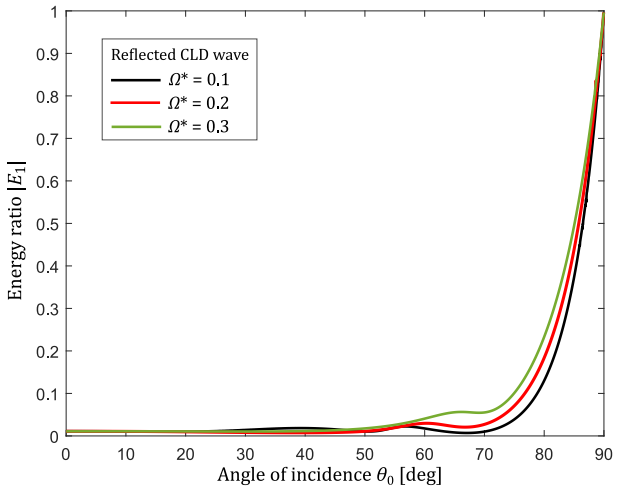

Fig. 8. Variations of the energy ratios of reflected coupled longitudinal displacement (CLD) wave against the angle of incidence of incident CLD wave for different values of rotation rate.

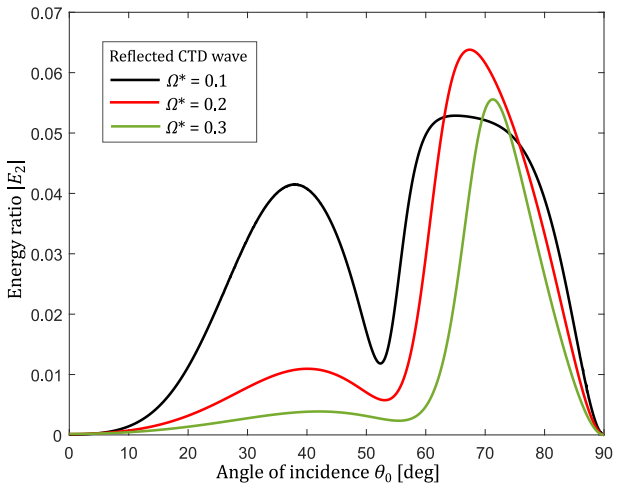

Fig. 9. Variations of the energy ratios of reflected coupled transverse displacement (CTD) wave against the angle of incidence of incident CLD wave for different values of rotation rate.

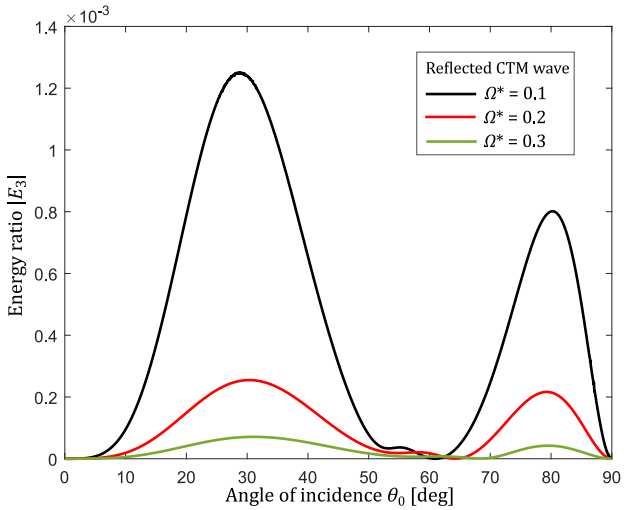

Fig. 10. Variations of the energy ratios of reflected coupled transverse microrotational (CTM) wave against the angle of incidence of incident CLD wave for different values of rotation rate.

Figure 11 illustrates the energy ratio variations of transmitted CLD waves against the angle of incidence for different values of rotation rate. For each value of rotation rate, the energy ratios are approximately one at normal incidence and then decrease logarithmically to a value zero at grazing incidence. The energy ratio variations of transmitted CTD and CTM waves are also shown graphically in Figs 12 and 13 against the angle of incidence for different values of rotation rate. For each value of rotation rate, the energy ratios for

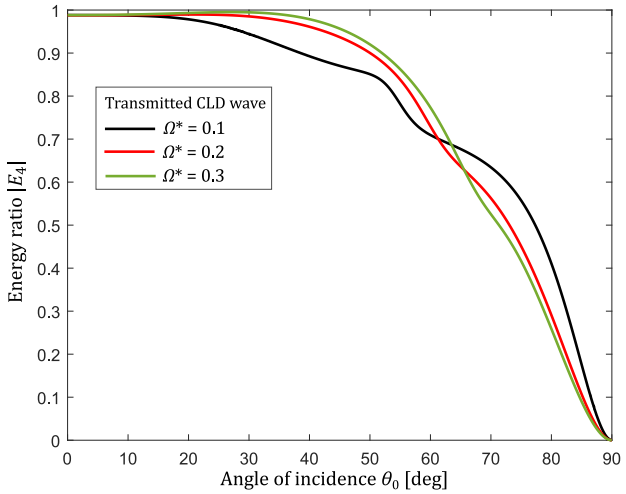

Fig. 11. Variations of the energy ratios of transmitted coupled longitudinal displacement (CLD) wave against the angle of incidence of incident CLD wave for different values of rotation rate.

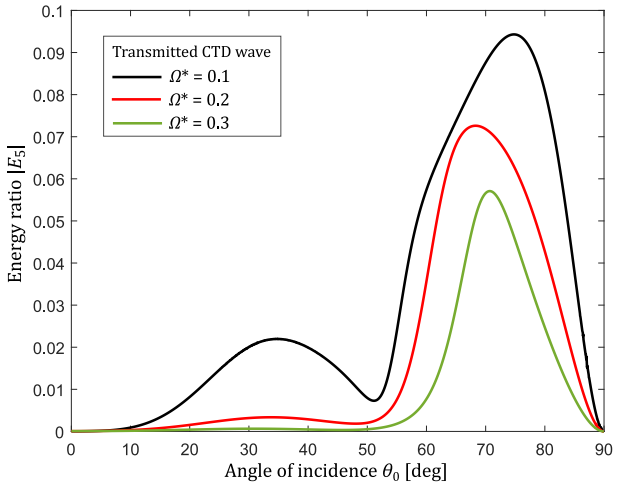

Fig. 12. Variations of the energy ratios of transmitted coupled transverse displacement (CTD) wave against the angle of incidence of incident CLD wave for different values of rotation rate.

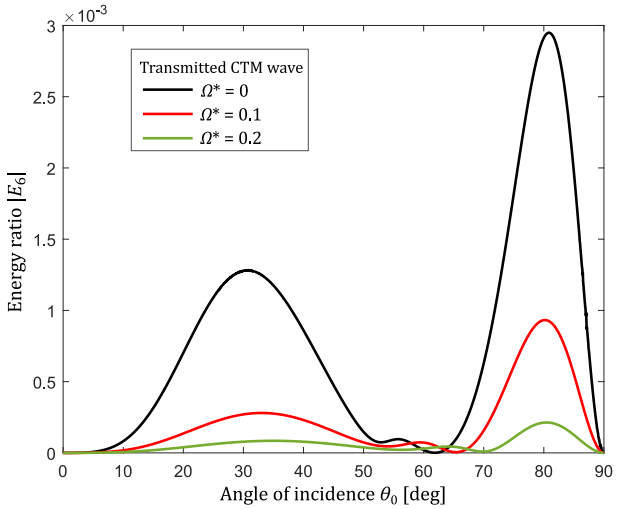

Fig. 13. Variations of the energy ratios of transmitted coupled transverse microrotational (CTM) wave against the angle of incidence of incident CLD wave for different values of rotation rate.

these waves are zero at normal and grazing incidences and oscillate at other angles.

From Figs 8 to 13, it can be noticed that the effect of rotation on the reflected and transmitted CLD, CTD and CTM waves is considerable at each angle of incidence except normal and grazing incidences.

6. Conclusion

A rotating model of two different transversely isotropic micropolar piezoelectric solid half-spaces in welded contact is considered for reflection and transmission of plane-waves. There exist three coupled plane-waves in a rotating and transversely micropolar piezoelectric medium. The nature of these three plane-waves depends on the axis of rotation and the propagation direction. The effects of rotation do not increase the number of waves in a micropolar piezoelectric medium, but it affects their speeds significantly. For an incident plane-wave, the connections between the amplitude ratios and the expressions for energy ratios are obtained. Based on a particular numerical example of the theoretical model, the effects of rotation are analyzed on the speeds and energy ratios of reflected and transmitted waves for an incident plane-wave. From the discussion of graphical illustrations, the following important theoretical observations are made:

1) The speed variations of reflected and transmitted waves vary in different manner against the angle of incidence. The presence of rotation changes the values of speed at each angle of incidence and does not affect the speed variations significantly against the angle of incidence.
2) The speeds of the transmitted waves are observed slower as compared to the speeds of reflected waves.
3) The sum of energy ratios of all reflected and transmitted waves is observed less than or equal one at each angle of incidence. This fact is helpful in validating the numerical results if simulations are not based an experimental data.
4) For incidence of CLD wave, the energy shares of reflected and transmitted CLD waves are found maximum. However, the energy shares of reflected and transmitted CTM waves are found much smaller as compared to other reflected and transmitted waves.
5) The energy ratios of all reflected and transmitted waves are also influenced by the rotation rate at each angle of incidence except normal and grazing incidences.

Wave propagation in micropolar piezoelectricity is quite a new and emerging area of research. Since the formulation of the linear theory of micropolar piezoelectricity, few papers on wave propagation in micropolar piezoelectric materials have appeared with theoretical predictions. Due to the non-availability of experimental values of micropolar piezoelectric constants, the numerical observations of the present paper are also of theoretical nature. However, the present numerical results on the energy ratios of reflected and transmitted waves are verified using energy conservation law. The present theoretical predictions with the effects of rotation on the speeds and energy ratios of reflected and transmitted waves may provide more relevant inputs for experimental researchers working on non-destructive evaluation (NDE) techniques for structural health monitoring and in development of new sensing devices of finite geometrical sizes.

Appendix 1

The expressions for H_s $(s = 0, 1, 2, 3)$ are given as

$$D_1 = A_{11}\sin^2\theta + A_{55}\cos^2\theta,$$

$$D_2 = A_{66}\sin^2\theta + A_{33}\cos^2\theta,$$

$$D_3 = \lambda_{15}\sin^2\theta + \lambda_{33}\cos^2\theta,$$

$$D_4 = B_{77}\sin^2\theta + B_{66}\cos^2\theta,$$

$$D_5 = \gamma_{11}\sin^2\theta + \gamma_{33}\cos^2\theta,$$

$$L_1 = (A_{13} + A_{56})\sin\theta\cos\theta,$$

$$L_2 = (\lambda_{15} + \lambda_{31})\sin\theta\cos\theta,$$

$$\Omega^* = \frac{\Omega}{\omega},$$

$$M_1 = \left[1 + (\Omega^*)^2\right]\rho\omega^2,$$

$$M_2 = 2i\rho\omega^2\Omega^*,$$

$$M_3 = \chi - \rho j\omega^2,$$

$$K_{11} = iK_1\cos\theta,$$

$$K_{22} = iK_2\sin\theta,$$

$$H_0 = D_5M_3\left(M_1^2 + M_2^2\right),$$

$$H_1 = D_5M_1M_3\left(D_1 + D_2\right) + D_5M_1\left(K_{11}^2 + K_{22}^2\right) + M_1M_3\left(D_3^2 + L_2^2\right) - D_4D_5\left(M_1^2 + M_2^2\right),$$

$$H_2 = \left(D_2D_5 + D_3^2\right)K_{11}^2 + \left(D_1D_5 + L_2^2\right)K_{22}^2 - 2\left(D_3L_2 + D_5L_1\right)K_{11}K_{22} - D_4M_1\left(D_3^2 + L_2^2\right) - D_4D_5M_1\left(D_1 + D_2\right) - 2D_3L_1L_2M_3 + \left(D_1D_3^2 + D_2L_2^2\right)M_3 + \left(D_1D_2 - L_1^2\right)D_5M_3,$$

$$H_3 = D_4D_5L_1^2 + 2D_3D_4L_1L_2 - D_1D_4D_3^2 - D_2D_4L_2^2 - D_1D_2D_4D_5.$$

Appendix 2

The expressions for ξ_o, η_o, ζ_o, ξ'_m, η'_m, ζ'_m, ξ_m, η_m, and ζ_m $(m = 1, 2, 3)$ using Snell's law are given as

$$\xi_o = \frac{\Delta_{01}}{\Delta_0}, \qquad \frac{\eta_o}{k'_1} = \frac{\Delta_{02}}{\Delta_0}, \qquad \zeta_o = \frac{\Delta_{03}}{\Delta_0},$$

$$\xi'_m = \frac{\Delta'_{1m}}{\Delta'_m}, \qquad \frac{\eta'_m}{k'_m} = \frac{\Delta'_{2m}}{\Delta'_m}, \qquad \zeta'_m = \frac{\Delta'_{3m}}{\Delta'_m},$$

$$\xi_m = \frac{\Delta_{1m}}{\Delta_m}, \qquad \frac{\eta_m}{k_m} = \frac{\Delta_{2m}}{\Delta_m}, \qquad \zeta_m = \frac{\Delta_{3m}}{\Delta_m},$$

where

$$\Delta_0 = \begin{vmatrix} C_0 & -K'_{11} & -S'_1 \\ Q'_1 & K'_{21} & F'_1 \\ K^{*'}_{21} & R'_1 & 0 \end{vmatrix}, \quad \Delta_{01} = \begin{vmatrix} P'_1 & -K'_{11} & -S'_1 \\ G_0 & K'_{21} & F'_1 \\ -K^{*'}_{11} & R'_1 & 0 \end{vmatrix},$$

$$\Delta_{02} = \begin{vmatrix} C_o & P'_1 & -S'_1 \\ Q'_1 & G_o & F'_1 \\ K^{*'}_{21} & -K^{*'}_{11} & 0 \end{vmatrix}, \quad \Delta_{03} = \begin{vmatrix} C_0 & -K'_{11} & P'_1 \\ Q'_1 & K'_{21} & G_o \\ K^{*'}_{21} & R'_1 & -K^{*'}_{11} \end{vmatrix},$$

$$\Delta'_m = \begin{vmatrix} C'_m & K'_{1m} & S'_m \\ Q'_m & K'_{2m} & F'_m \\ K^{*'}_{2m} & R'_m & 0 \end{vmatrix}, \quad \Delta'_{1m} = \begin{vmatrix} P'_m & K'_{1m} & S'_m \\ G'_m & K'_{2m} & F'_m \\ K^{*'}_{1m} & R'_m & 0 \end{vmatrix},$$

$$\Delta'_{2m} = \begin{vmatrix} C'_m & P'_m & S'_m \\ Q'_m & G'_m & F'_m \\ K^{*'}_{2m} & K^{*'}_{1m} & 0 \end{vmatrix}, \quad \Delta'_{3m} = \begin{vmatrix} C'_m & K'_{1m} & P'_m \\ Q'_m & K'_{2m} & G'_m \\ K^{*'}_{2m} & R'_m & K^{*'}_{1m} \end{vmatrix},$$

$$\Delta_m = \begin{vmatrix} C_m & K_{1m} & S_m \\ Q_m & K_{2m} & F_m \\ K^*_{2m} & R_m & 0 \end{vmatrix}, \quad \Delta_{1m} = \begin{vmatrix} P_m & K_{1m} & S_m \\ G_m & K_{2m} & F_m \\ K^*_{1m} & R_m & 0 \end{vmatrix},$$

$$\Delta_{2m} = \begin{vmatrix} C_m & P_m & S_m \\ Q_m & G_m & F_m \\ K^*_{2m} & K^*_{1m} & 0 \end{vmatrix}, \quad \Delta_{3m} = \begin{vmatrix} C_m & K_{1m} & P_m \\ Q_m & K_{2m} & G_m \\ K^*_{2m} & R_m & K^*_{1m} \end{vmatrix},$$

$$P'_m = \left[1 + (\Omega^*)^2\right]\rho' v'^2_m - A'_{11}\sin^2\theta_o\left(\frac{v'_m}{v'_1}\right)^2 - A'_{55}\left[1 - \sin^2\theta_o\left(\frac{v'_m}{v'_1}\right)^2\right],$$

$$Q'_m = \left[1 + (\Omega^*)^2\right]\rho' v'^2_m - A'_{66}\sin^2\theta_o\left(\frac{v'_m}{v'_1}\right)^2 - A'_{33}\left[1 - \sin^2\theta_o\left(\frac{v'_m}{v'_1}\right)^2\right],$$

$$R'_m = \frac{B'_{77}}{j'}\sin^2\theta_o\left(\frac{v'_m}{v'_1}\right)^2 + \frac{B'_{66}}{j'}\left[1 - \sin^2\theta_o\left(\frac{v'_m}{v'_1}\right)^2\right] + \frac{\chi'}{j'k'^2_m} - \rho' v'^2_m,$$

$$F'_m = \lambda'_{15}\sin^2\theta_o\left(\frac{v'_m}{v'_1}\right)^2 + \lambda'_{33}\left[1 - \sin^2\theta_o\left(\frac{v'_m}{v'_1}\right)^2\right],$$

$$C'_m = -\left[(A'_{13} + A'_{56})\sin\theta_o\left(\frac{v'_m}{v'_1}\right) \cdot \sqrt{1 - \sin^2\theta_o\left(\frac{v'_m}{v'_1}\right)^2} + 2i\Omega^*\rho' v'^2_m\right],$$

$$C_o = (A'_{13} + A'_{56}) \sin\theta_o \cos\theta_o - 2i\Omega^* \rho' v_1'^2,$$

$$G'_m = \left[-(A'_{13} + A'_{56}) \sin\theta_o \left(\frac{v'_m}{v'_1}\right) \cdot \sqrt{1 - \sin^2\theta_o \left(\frac{v'_m}{v'_1}\right)^2} + 2i\Omega^* \rho' v_m'^2 \right],$$

$$G_o = (A'_{13} + A'_{56}) \sin\theta_o \cos\theta_o + 2i\Omega^* \rho' v_1'^2,$$

$$S'_m = (\lambda'_{15} + \lambda'_{31}) \sin\theta_o \left(\frac{v'_m}{v'_1}\right) \sqrt{1 - \sin^2\theta_o \left(\frac{v'_m}{v'_1}\right)^2},$$

$$K'_{1m} = iK'_1 \sqrt{1 - \sin^2\theta_o \left(\frac{v'_m}{v'_1}\right)^2},$$

$$K'_{2m} = iK'_2 \sin\theta_o \left(\frac{v'_m}{v'_1}\right),$$

$$K^{*'}_{1m} = \frac{K'_{1m}}{j' k_m'^2} K^{*'}_{2m} = \frac{K'_{2m}}{j' k_m'^2},$$

$$P_m = \left[1 + (\Omega^*)^2\right] \rho v_m^2 - A_{11} \sin^2\theta_o \left(\frac{v_m}{v'_1}\right)^2 - A_{55} \left[1 - \sin^2\theta_o \left(\frac{v_m}{v'_1}\right)^2\right],$$

$$Q_m = \left[1 + (\Omega^*)^2\right] \rho v_m^2 - A_{66} \sin^2\theta_o \left(\frac{v_m}{v'_1}\right)^2 - A_{33} \left[1 - \sin^2\theta_o \left(\frac{v_m}{v'_1}\right)^2\right],$$

$$R_m = \frac{B_{77}}{j} \sin^2\theta_o \left(\frac{v_m}{v'_1}\right)^2 + \frac{B_{66}}{j} \left[1 - \sin^2\theta_o \left(\frac{v_m}{v'_1}\right)^2\right] + \frac{\chi}{jk_m^2} - \rho v_m^2,$$

$$F_m = \lambda_{15} \sin^2\theta_o \left(\frac{v_m}{v'_1}\right)^2 + \lambda_{33} \left[1 - \sin^2\theta_o \left(\frac{v_m}{v'_1}\right)^2\right],$$

$$C_m = (A_{13} + A_{56}) \sin\theta_0 \left(\frac{v_m}{v'_1}\right) \sqrt{1 - \sin^2\theta_o \left(\frac{v_m}{v'_1}\right)^2} - 2i\Omega^* \rho v_m^2,$$

$$G_m = (A_{13} + A_{56}) \sin\theta_o \left(\frac{v_m}{v'_1}\right) \sqrt{1 - \sin^2\theta_o \left(\frac{v_m}{v'_1}\right)^2} + 2i\Omega^* \rho v_m^2,$$

$$S_m = -(\lambda_{15} + \lambda_{31}) \sin\theta_o \left(\frac{v_m}{v'_1}\right) \sqrt{1 - \sin^2\theta_o \left(\frac{v_m}{v'_1}\right)^2},$$

$$K_{1m} = -iK_1 \sqrt{1 - \sin^2\theta_o \left(\frac{v_m}{v'_1}\right)^2},$$

$$K_{2m} = iK_2 \sin\theta_o \left(\frac{v_m}{v'_1}\right),$$

$$K^*_{1m} = \frac{K_{1m}}{jk_m^2},$$

$$K^*_{2m} = \frac{K_{2m}}{jk_m^2},$$

$$\Omega^* = \frac{\Omega}{\omega}.$$

References

1. Achenbach J.D. (1973), *Wave Propagation in Elastic Solids*, Vol. 16, North-Holland Publishing Company, Elsevier, Amsterdam.
2. Alshits V.I., Lothe J., Lyubimov V.N. (1984), The phase shift for reflection of elastic waves in hexagonal piezoelectric crystals, *Wave Motion*, **6**(3): 259–264, doi: 10.1016/0165-2125(84)90029-5.
3. Alshits V.I., Shuvalov A.L. (1995), Resonance reflection and transmission of shear elastic waves in multilayered piezoelectric structures, *Journal of Applied Physics*, **77**(6): 2659–2665, doi: 10.1063/1.358732.
4. Aouadi M. (2008), Aspects of uniqueness in micropolar piezoelectric bodies, *Mathematics and Mechanics of Solids*, **13**: 499–512, doi: 10.1177%2F1081286507077106.
5. Auld B.A. (1973), *Acoustic Fields and Waves in Solids*, Wiley Interscience, New York.
6. Auld B.A. (1981), Wave propagation and resonance in piezoelectric materials, *The Journal of the Acoustical Society of America*, **70**(6): 1577–1585, doi: 10.1121/1.387223.
7. Barati M.R., Zenkour A.M. (2018), Electrothermoelastic vibration of plates made of porous functionally graded piezoelectric materials under various boundary conditions, *Journal of Vibration and Control*, **24**(10): 1910–1926, doi: 10.1177%2F1077546316672788.
8. Burkov S.I., Sorokin B.P., Aleksandrov K.S., Karpovich A.A. (2009), Reflection and refraction of bulk acoustic waves in piezoelectrics under uniaxial stress, *Acoustical Physics*, **55**: 178–185, doi: 10.1134/S1063771009020055.
9. Cheng N.C., Sun C.T. (1975), Wave propagation in two-layered piezoelectric plates, *The Journal of the Acoustical Society of America*, **57**(3): 632–638, doi: 10.1121/1.380479.

10. Ciumasu S.G., Vieru D. (1999), Variational formulations for the vibration of a micropolar piezoelectric body, *The Journal of the Acoustical Society of America*, **105**(2): 1240, doi: 10.1121/1.425960.

11. Cracium I.A. (1995), Uniqueness theorem in the linear theory of piezoelectric micropolar thermoelasticity, *International Journal of Engineering Science*, **33**: 1027–1036, doi: 10.1016/0020-7225(94)00106-T.

12. Darinskii A.N., Clezio E.L., Feuillard G. (2008), The role of electromagnetic waves in the reflection of acoustic waves in piezoelectric crystals, *Wave Motion*, **45**(4): 428–444, doi: 10.1016/j.wavemoti.2007.08.001.

13. Ergin K. (1950), Energy ratio of the seismic waves reflected and refracted at a rock-water boundary, *Bulletin of the Seismological Society of America*, **42**(4): 349–372, doi: 10.1785/BSSA0420040349.

14. Eringen A.C. (1966), Linear theory of micropolar elasticity, *Journal of Mathematics and Mechanics*, **15**(6): 909–923, https://www.jstor.org/stable/24901442.

15. Eringen A.C. (1968), *Theory of Micropolar Elasticity in Fracture*, Vol. 2, Academic Press, pp. 621–729.

16. Eringen A.C. (1999), *Microcontinuum Field Theories I: Foundations and Soilds*, Springer, New York.

17. Every A.G., Neiman V.I. (1992), Reflection of electroacoustic waves in piezoelectric solids: Mode conversion into four bulk waves, *Journal of Applied Physics*, **71**(12): 6018–6024, doi: 10.1063/1.350457.

18. Ewing W.M., Jardetzky W.S., Press F. (1957), *Elastic Waves in Layered Media*, McGraw-Hill Company Inc., New York, Toronto, London.

19. Gales C. (2012), Some results in micromorphic piezoelectricity, *European Journal of Mechanics- A/Solids*, **31**(1): 37–46, doi: 10.1016/j.euromechsol.2011.06.014.

20. Guo X., Wei P. (2014), Effects of initial stress on the reflection and transmission waves at the interface between two piezoelectric half spaces, *International Journal of Solids and Structures*, **51**(21–22): 3735–3751, doi: 10.1016/j.ijsolstr.2014.07.008.

21. Guo X., Wei P., Li L., Tang Q. (2015), Influences of mechanically and dielectrically imperfect interfaces on the reflection and transmission waves between two piezoelectric half spaces, *International Journal of Solids and Structures*, **63**: 184–205, doi: 10.1016/j.ijsolstr.2015.02.050.

22. Gutenberg B. (1944), Energy ratio of reflected and refracted seismic waves, *Bulletin of the Seismological Society of America*, **34**(2): 85–102, doi: 10.1785/BSSA0340020085.

23. Hruska K. (1966), The rate of propagation of ultrasonic waves in ADP in Voigt's theory, *Czechoslovak Journal of Physics B*, **16**(5): 446–454, doi: 10.1007/BF01696256.

24. Iesan D. (2006), On the microstretch piezoelectricity, *International Journal of Engineering Science*, **44**(13–14): 819–829, doi: 10.1016/j.ijengsci.2006.05.007.

25. Jeffreys H. (1926), The reflexion and refraction of elastic waves, *Geophysical Supplements to the Monthly Notices of the Royal Astronomical Society*, **1**(7): 321–334, doi: 10.1111/j.1365-246X.1926.tb05380.x.

26. Jiao F., Wei P., Zhou Y., Zhou X. (2019), Wave propagation through a piezoelectric semiconductor slab sandwiched by two piezoelectric half-spaces, *European Journal of Mechanics-A/Solids*, **75**: 70–81, doi: 10.1016/j.euromechsol.2019.01.007.

27. Kaung Z.B. (2013), *Theory of Electroelasticity*, Springer.

28. Knott C.G. (1899), Reflexion and refraction of elastic waves with seismological applications, *The London, Edinburgh, and Dublin Philosophical Magazine and Journal of Science*, **48**: 64–97, doi: 10.1080/14786449908621305.

29. Kuang Z.B., Yuan X.G. (2011), Reflection and transmission of waves in pyroelectric and piezoelectric materials, *Journal of Sound and Vibration*, **330**(6): 1111–1120, doi: 10.1016/j.jsv.2010.09.026.

30. Kyame J.J. (1949), Wave propagation in piezoelectric crystals, *The Journal of the Acoustical Society of America*, **21**(3): 159–167, doi: 10.1121/1.1906490.

31. Liu C., Yu J., Wang X., Zhang B., Zhang X., Zhou H. (2021), Reflection and transmission of elastic waves through nonlocal piezoelectric plates sandwiched in two solid half-spaces, *Thin-Walled Structures*, **168**: 108306, doi: 10.1016/j.tws.2021.108306.

32. Othman M.I.A., Elmaklizi Y.D., Ahmed E.A.A. (2017a), Effect of magnetic field on piezo-thermoelastic medium with three theories, *Results in Physics*, **7**: 361–3368, doi: 10.1016/j.rinp.2017.08.058.

33. Othman M.I.A., Elmaklizi Y.D., Ahmed E.A.A. (2017b), Influence of magnetic field on generalized piezo-thermoelastic rotating medium with two relaxation times, *Microsystem Technologies*, **23**, 5599–5612, doi: 10.1007/s00542-017-3513-7.

34. Pailloux P.M.H. (1958), Piezoelectricity. Calculation of propagation velocities [in French: Piézoélectricité. Calcul des vitesses de propagation], *Le Journal De Physique Etle Radium*, **19**(5): 523–526, doi: 10.1051/jphysrad:01958001905052300.

35. Pal M.K., Singh A.K. (2021), Analysis of reflection and transmission phenomenon at distinct bonding interfaces in a rotating pre-stressed functionally graded piezoelectric-orthotropic structure, *Applied Mathematics and Computation*, **409**: 126398, doi: 10.1016/j.amc.2021.126398.

36. Pang Y., Wang Y.S., Liu J.X, Fang D.N. (2008), Reflection and refraction of plane waves at the interface between piezoelectric and piezomagnetic media, *International Journal of Engineering Science*, **46**(11): 1098–1110, doi: 10.1016/j.ijengsci.2008.04.006.

37. Parafitt V.R., Eringen A.C. (1969) Reflection of plane waves from the flat boundary of a micropolar elastic half-space, *The Journal of the Acoustical Society of America*, **45**(5): 1258–1272, doi: 10.1121/1.1911598.

38. Parton V.Z., Kudryavtsev B.A. (1988), *Electromagnetoelasticity: Piezoelectrics and Electrically Conductive Solids*, Gordon and Beach, New York.

39. Rosenbaum J.F. (1988), *Bulk Acoustic Wave Theory and Devices*, Artech House, Boston.

40. Sahu S.A., Nirwal S., Mondal S. (2021), Reflection and transmission of quasi-plane waves at the interface of piezoelectric semiconductors with initial stresses, *Applied Mathematics and Mechanics*, **42**(7): 951–968, doi: 10.1007/s10483-021-2738-9.

41. Sangwan A., Singh B., Singh J. (2018), Reflection and transmission of plane waves at an interface between elastic and micropolar piezoelectric solid half-spaces, *Technische Mechanik*, **38**(3): 267–285, doi: 10.24352/UB.OVGU-2018-034.

42. Schoenberg M., Censor D. (1973), Elastic waves in rotating media, *Quarterly of Applied Mathematics*, **31**(1): 115–125, doi: 10.1090/qam/99708.

43. Singh B. (2010), Wave propagation in a prestressed piezoelectric half-space, *Acta Mechanica*, **211**(3): 337–344, doi: 10.1007/s00707-009-0234-8.

44. Singh B. (2013), Propagation of shear waves in a piezoelectric medium, *Mechanics of Advanced Materials and Structures*, **20**(6): 434–440, doi: 10.1080/15376494.2011.627633.

45. Singh B., Sangwan A., Singh J. (2019), Reflection and transmission of elastic waves at an interface between two micropolar piezoelectric half-spaces, *Journal of Ocean Engineering and Science*, **4**(3): 227–237, doi: 10.1016/j.joes.2019.04.006.

46. Singh B., Sindhu R. (2016), On propagation of Rayleigh type surface wave in a micropolar piezoelectric medium, *Open Journal of Acoustics*, **6**(4): 35–44, doi: 10.4236/oja.2016.64004.

47. Singh B., Sindhu R. (2018), Rotational effects on propagation of Rayleigh wave in a micropolar piezoelectric medium, *Journal of Theoretical and Applied Mechanics, Sofia*, **48**(2): 93–105, doi: 10.2478/jtam-2018-0012.

48. Singh S., Singh A.K., Guha S. (2021), Impact of interfacial imperfections on the reflection and transmission phenomenon of plane waves in a porous-piezoelectric model, *Applied Mathematical Modelling*, **100**: 656–675, doi: 10.1016/j.apm.2021.08.022.

49. Tiersten H.F., Stevens D.S., Das P.K. (1980), Acoustic surface wave accelerometer and rotation rate sensor, [in:] *Proceedings of IEEE Ultrasonics Symposium*, pp. 692–695, doi: 10.1109/ULTSYM.1980.197488.

50. Tiersten H.F., Stevens D.S., Das P.K. (1981), Circulating flexural wave rotation rate sensor, [in:] *Proceedings of IEEE Ultrasonics Symposium*, pp. 163–166, doi: 10.1109/ULTSYM.1981.197602.

51. Vieru D., Ciumasu S.G. (1999), Love waves in nonclassical micropolar piezoelectricity, *The Journal of the Acoustical Society of America*, **105**(2): 1241, doi: 10.1121/1.426640.

52. White R.W. (1998), Acoustic sensors for physical, chemical and biochemical applications, [in:] *Proceedings of the 1998 IEEE International Frequency Control Symposium (Cat. No.98CH36165)*, pp. 587–594, doi: 10.1109/FREQ.1998.717960.

53. Wren T., Burdess J. S. (1987), Surface waves perturbed by rotation, *ASME Journal of Applied Mechanics*, **54**(2): 464–466, doi: 10.1115/1.3173043.

54. Xue B. *et al.* (2012), Photo-induced effects in GeS2 glass and glass–ceramics stimulated by green and IR lasers, *Materials Letters*, **73**: 14–16, doi: 10.1016%2Fj.matlet.2011.12.089.

55. Yuan X., Zhu Z.H. (2012), Reflection and refraction of plane waves at interface between two piezoelectric media, *Acta Mechanica*, **223**(12): 2509–2521, doi: 10.1007/s00707-012-0728-7.

56. Zenkour A.M., Alghanmi R.A. (2019a), Bending of exponentially graded plates integrated with piezoelectric fiber-reinforced composite actuators resting on elastic foundations, *European Journal of Mechanics-A/Solids*, **75**: 461–471, doi: 10.1016/j.euromechsol.2019.03.003.

57. Zenkour A.M., Alghanmi R.A. (2019b), Stress analysis of a functionally graded plate integrated with piezoelectric faces via a four-unknown shear deformation theory, *Results in Physics*, **12**: 268–277, doi: 10.1016/j.rinp.2018.11.045.

58. Zenkour A.M., Alghanmi R.A. (2020), Static response of sandwich plates with FG core and piezoelectric faces under thermo-electro-mechanical loads and resting on elastic foundations, *Thin-Walled Structures*, **157**: 107025, doi: 10.1016/j.tws.2020.107025.

59. Zenkour A.M., Aljadani M.H. (2019), Porosity effect on thermal buckling behavior of actuated functionally graded piezoelectric nanoplates, *European Journal of Mechanics-A/Solids*, **78**: 103835, doi: 10.1016/j.euromechsol.2019.103835.

60. Zenkour A.M., Aljadani M.H. (2020), Buckling analysis of actuated functionally graded piezoelectric plates via a quasi-3D refined theory, *Mechanics of Materials*, **151**: 103632, doi: 10.1016/j.mechmat.2020.103632.

61. Zenkour A.M., Hafed Z.S. (2019), Hygro-thermo-mechanical bending of FG piezoelectric plates using quasi-3D shear and normal deformations theory, *Latin American Journal of Solids and Structures*, **16**(7): e218, doi: 10.1590/1679-78255396.

62. Zenkour A.M., Hafed Z.S. (2020a), Bending analysis of functionally graded piezoelectric plates via quasi-3D trigonometric theory, *Mechanics of Advanced Materials and Structures*, **27**(18): 1551–1562, doi: 10.1080/15376494.2018.1516325.

63. Zenkour A.M., Hafed Z.S. (2020b), Bending response of functionally graded piezoelectric plates using a two-variable shear deformation theory, *Advances in Aircraft and Spacecraft Science*, **7**(2): 115–134, doi: 10.12989/aas.2020.7.2.115.

64. Zhilin P.A., Kolpakov Y.E. (2005), A micro-polar theory for piezoelectric materials, [in:] *Proceedings of the Advanced Problems in Mechanics*, Lecture at XXXIII Summer School – Conference, St. Petersburg, Russia, http://mathenglish.ru/mechanics/zhilin/zhilin8.pdf.